Strong-field approximation for Coulomb explosion of H_2^+ and D_2^+ by short intense laser pulses

H. A. Leth,[1] L. B. Madsen,[1] and J. F. McCann[2]

[1]*Lundbeck Foundation Theoretical Center for Quantum System Research, Department of Physics and Astronomy, University of Aarhus, 8000 Århus C, Denmark*

[2]*Centre for Theoretical Atomic Molecular and Optical Physics, School of Mathematics and Physics, Queen's University Belfast, Belfast BT7 1NN, United Kingdom*

(Received 18 April 2007; revised manuscript received 25 June 2007; published 24 September 2007)

We present a simple quantum mechanical model to describe Coulomb explosion of H_2^+ and D_2^+ by short, intense infrared laser pulses. The model is based on the length gauge version of the molecular strong-field approximation and is valid when the process of dissociation prior to ionization is negligible. The results are compared with recent experimental data for the proton kinetic energy spectrum [Th. Ergler *et al.*, Phys. Rev. Lett. **95**, 093001 (2005); D. S. Murphy *et al.*, J. Phys. B **40**, S359 (2007)]. Using a Franck-Condon distribution over initial vibrational states, the theory reproduces the overall shape of the spectrum with only a small overestimation of slow protons. The agreement between theory and experiment can be made perfect by using a non-Frank-Condon initial distribution characteristic for H_2^+ (D_2^+) targets produced by strong-field ionization of H_2 (D_2). For comparison, we also present results obtained by two different tunneling models for this process.

DOI: 10.1103/PhysRevA.76.033414 PACS number(s): 32.80.Rm, 33.80.Rv

I. INTRODUCTION

Ultrashort, highly intense, laser pulses at infrared wavelengths are currently being used to study molecular dynamics under extreme conditions. These systems are commonly based upon a Ti:sapphire laser, tunable around 790 nm, which can reach peak intensities in the range $10^{13}-10^{17}$ W/cm^2, with pulse lengths shorter than 50 fs. Consequently energy can be deposited on time scales shorter than the fastest molecular vibration with field strengths comparable to the molecular bond. When molecules are exposed to such an environment, the response is highly-nonlinear and generally leads to multiple dissociative ionization and high-order optical scattering. Indeed the multiple fragmentation process for a heavy polyatomic multielectron system prevents a detailed analysis of the energy transfer, simply due to the proliferation of fragments produced. Small molecular systems, on the other hand, have simpler structure and fewer relaxation channels. Moreover, the fundamental molecules such as H_2 or D_2 have an intrinsic value owing to their relatively fast vibration. Since a 790 nm pulse has a cycle period of 2.6 fs, and perhaps 10–50 fs duration, the vibration provides an additional internal clock that records the response of the electronic excitation during the passage of the pulse. Consequently, there has been extensive study of the interaction of intense field dissociative ionization of H_2 (D_2) and H_2^+ (D_2^+) with progressively shorter and more intense pulses and, in particular, using the ejected proton kinetic energy spectrum as an indicator of the electron response and a diagnostic of the pulse itself. For reviews of progress in this field one can consult, for example, Refs. [1–3].

In analyzing the ionization dynamics of H_2^+ (D_2^+) in strong laser pulses it is helpful to make a division into two regimes determined by the duration of the pulse τ in comparison with the time scale for the vibrational motion, T_{vib} ($T_{\mathrm{vib}} \simeq 15$ fs for H_2^+; $T_{\mathrm{vib}} \simeq 24$ fs for D_2^+). When $\tau \gg T_{\mathrm{vib}}$ the pulse is "long" and there is time for nuclear dynamics during the pulse. Oppositely, when $\tau \ll T_{\mathrm{vib}}$ the pulse is "short" and there is no time for the nuclei to move considerably while the field is on. In the long pulse regime the single-proton kinetic energy spectrum is dominated by proton energies below 4 eV with a characteristic peak at 2–3 eV. The repulsive $1/R$ curve for the nuclear coordinate R allows a direct mapping between the kinetic energy release and the nuclear distance at the instant of ionization and the energies observed indicate that the ionization peaks at internuclear distances larger than the equilibrium distance. Theoretically this can be explained by nuclear motion and the effects of charge-resonance enhanced ionization [4] and dynamic tunneling ionization [5]. For recent experiments in this regime see, e.g., Refs. [6–15].

In the "short" pulse regime the duration of the pulse is, say, up to $\sim 2T_{\mathrm{vib}}$ leaving not much time for the heavy nuclei to move during the peak of the pulse. This means that ionization takes place also from the equilibrium distance and consequently larger kinetic energy releases are observed [16–22].

In this work, we present a simple quantum mechanical model designed to predict the single-proton kinetic energy spectrum of dissociative ionization of H_2^+ in the "short" pulse regime. We use the strong-field approximation (SFA) within the length gauge [23,24]. That is, we calculate transition rates from a molecular state, in which the laser field is neglected, to a state in which the laser field is accounted for to all orders, but some approximations are made for the three-body continuum. The calculations are simplified by assuming the Born-Oppenheimer separation of motions, and the Franck-Condon principle is invoked for the nuclear motion. These approximations allow us to determine the dissociative ionization *rates* to different channels in a simple way. The pulse is presented by a Fourier expansion so that the temporal intensity variation is taken into account. This averaging is important due to the ponderomotive shift of the electron which may cause channel closings when the intensity is raised.

Following this procedure, and integrating over the electron spectrum, the proton energy distribution can be obtained. Taking into account the non-Frank-Condon distribution over vibrational states typical for molecular ions produced by strong-field ionization [25–27] we obtain very good agreement between the model predictions and experimental data [17,22]. Finally, for completion, we compare the predictions of our model with tunneling theory calculations. Atomic units ($|e|=\hbar=m_e=a_0=1$) are used throughout unless indicated otherwise.

II. MODEL

We consider the transition from a bound initial field-free state to a final continuum state in which the electron is only affected by the laser light, and the two protons are only subject to their mutual Coulomb repulsion. There are three essential elements of the model. First, the initial state, in which the vibrational population distribution plays a key role. Second, the overlap of these vibrational states with the final Coulomb states of the proton pair is of great importance in modulating the proton spectrum. Third, and most importantly, the coupling to the continuum, the nonpertubative photoionization rate, as a function of bond length and laser intensity will determine the range of proton energies. All three factors are intrinsically linked.

Consider a monochromatic plane-wave component of the light field, with linear polarization, $\hat{z}$, and angular frequency ω so that the vector potential in the dipole-approximation is

$$\boldsymbol{A}(t) = A_0 \hat{z} f(t) \cos \omega t, \tag{1}$$

where A_0 is the field amplitude, and the pulse shape is described by the factor, $0 \le f(t) \le 1$, which we take to be a Gaussian profile.

A. Molecular states

The process of formation of H_2^+ (D_2^+) requires ionization of the neutral species. The molecular ion H_2^+ (D_2^+) has only a single bound electronic state ($1s\sigma_g$) that is exactly known. The nuclear relaxation that follows this primary ionization is not so well defined and remains a source of uncertainty and investigation [3]. Nonetheless, to a very good approximation, the rotational degrees of freedom can be considered as frozen since its characteristic time scale $\gtrsim 170$ fs is much longer than the pulse duration. However, this results in an ensemble of vibrational modes, as observed in experiment [28]. As usual, the z axis of the laboratory reference frame is defined by the polarization vector, while the z axis of the molecular (body-fixed) frame is defined by the internuclear axis. The notation for the coordinates is that $\boldsymbol{R}$ denotes the internuclear vector and the electron coordinate with respect to the internuclear midpoint, is denoted by $\boldsymbol{r}$. In the following presentation, for consistency, the laboratory reference frame is employed. If we let ν denote the vibrational quantum number, then the eigenstates of the initial ensemble can be expressed as

$$\Psi_{i\nu}(\boldsymbol{R},\boldsymbol{r},t) = \phi_i(\boldsymbol{r},\boldsymbol{R}) \chi_{i\nu}(R) e^{-iE_{i\nu}t}, \tag{2}$$

where $\phi_i(\boldsymbol{r},\boldsymbol{R})$ is the electronic wave function, with energy $\varepsilon_i(R)$, and $\chi_{i\nu}(R)$ is the vibrational eigenfunction with eigenvalue $E_{Ni\nu}$. The total energy is then $E_{i\nu}=\varepsilon_i(R_0)+E_{Ni\nu}$. Recall that the electronic function has a σ_g^+ symmetry, and the transformation of $\phi_i(\boldsymbol{r},\boldsymbol{R})$ from laboratory to molecule frame is effected by the Wigner D rotation matrix [29,30].

In the final state, given the large separation between the nuclei and the electron at the time of ionization, we suppose that the influence of the protons on the electron is negligible compared to that of the external field [24]. This is consistent with the asymptotic ($t \to +\infty$) limit of the system as a (decoupled) product state of an outgoing Volkov wave ϕ_f (electron in the electromagnetic field) and a Coulomb wave χ_f for the proton motion:

$$\Psi_f(R,\boldsymbol{r},t) = \phi_f(\boldsymbol{r},t) \chi_f(R,t). \tag{3}$$

For an electron in a laser field described by Eq. (1), the length-gauge Hamiltonian is given by

$$H_f^{\mathrm{elec}} = \frac{p^2}{2} + \boldsymbol{r} \cdot \boldsymbol{F}, \tag{4}$$

where $\boldsymbol{p}$ is the canonical momentum and $\boldsymbol{F}=-\partial_t \boldsymbol{A}$ represents the electric field. The Volkov states form a complete set of solutions to the equation $i\partial_t \phi_f(\boldsymbol{r},t)=H_f^{\mathrm{elec}} \phi_f(\boldsymbol{r},t)$ and can be written

$$\phi_f(\boldsymbol{r},t) = \exp\left[i\boldsymbol{k}(t) \cdot \boldsymbol{r} - i \int_{-\infty}^{t} \frac{\boldsymbol{k}(t')^2}{2} dt' \right], \tag{5}$$

where $\boldsymbol{k}(t)=\boldsymbol{q}+\boldsymbol{A}(t)$ with $\boldsymbol{q}$ the kinematic momentum corresponding to a drift energy $q^2/2$, and where we denote the ponderomotive energy as $U_p=A_0^2/4$.

Since vibrational energies are much larger than rotational energies, and Coriolis coupling can be neglected at these energies, we make the usual assumption that the proton ejection occurs along the internuclear axis direction without rotation: the axial recoil approximation. Thus the nuclear motion is governed by the one-dimensional Coulomb repulsion:

$$H_f^{\mathrm{nucl}} = -\frac{1}{2\mu} \frac{\partial^2}{\partial R^2} + \frac{1}{R}, \tag{6}$$

where $\mu=\frac{1}{2}m_p$ is the reduced mass. The corresponding eigenfunction, with energy E_{Nf}, and wave number, $K_f=\sqrt{2\mu E_{Nf}}$, has the form

$$\chi_f(R) = \sqrt{\frac{2\mu}{\pi K_f}} F_0\left(\frac{\mu}{K_f}; K_f R \right), \tag{7}$$

where

$$F_0\left(\frac{\mu}{K_f}; K_f R \right) = e^{-(\pi/2)(\mu/K_f)+iK_f R} \left| \Gamma\left(1 + i\frac{\mu}{K_f} \right) \right| K_f R \times {}_1F_1\left(1 + i\frac{\mu}{K_f}; 2; -2iK_f R \right), \tag{8}$$

and ${}_1F_1$ is the confluent hypergeometric series. Since the Volkov wave represents all orders of the field amplitude, the

final state is a coherent sum of the full spectrum of photoelectron harmonics, including the angular distribution. Since our primary interest here is the comparison with experiment for the proton energy spectrum, we do not present results for the photoelectron differential yields. Instead we must integrate over these degrees of freedom. Furthermore, the initial vibrational state is a mixed state and the orientation of the molecule is random. In all, this amounts to integrating over four continuous variables and summing over two discrete variables, in addition to the matrix element calculation. However, since numerical quadrature is inherently a set of independent calculations, these calculations can readily be performed on a parallel computer.

B. Transition rates

To derive the expression for the transition amplitude, we follow the procedure of Ref. [31], and generalize to the case of an incoherent mixture of initial vibrational states each populated with probability P_ν. In this way we obtain the rate w for a transition into the final state Ψ_f of Eq. (3),

$$w = \sum_\nu P_\nu \sum_{n=n_0}^{\infty} 2\pi\delta(E_f - E_{i\nu} - n\omega)|A_{\nu n}|^2, \tag{9}$$

where

$$A_{\nu n} = \frac{1}{T}\int_0^T \langle \Psi_f | \boldsymbol{r}\cdot\boldsymbol{F} | \Psi_{i\nu}\rangle dt, \tag{10}$$

and the minimum number of photons absorbed, n_0, is determined by energy conservation. For a given number of absorbed photons, n, the electron momentum is defined as

$$q = \sqrt{2(E_{i\nu} + n\omega - U_p - E_{Nf})}. \tag{11}$$

To obtain the dissociative ionization rate, we multiply by the density of states per unit energy, per unit solid angle. Using the normalization convention defined above, the appropriate factor is $(2\pi)^{-3}q^2\, d\hat{\boldsymbol{q}}$. So that we have

$$\frac{dw}{dE_{Nf}} = \sum_\nu P_\nu \int d\hat{\boldsymbol{q}} \sum_{n=n_0}^{\infty} \frac{q}{(2\pi)^2}|A_{\nu n}|^2, \tag{12}$$

where $d\hat{\boldsymbol{q}}$ defines the direction of the outgoing electron.

The calculation of $A_{\nu n}(\boldsymbol{q})$ is significantly simplified in the Franck-Condon approximation, where it is assumed that the electronic transition appears almost instantaneously compared to changes in the nuclear position. That is, we can make the integration over the electron coordinate independent of the nuclear coordinate by replacing R by some fixed value R_0,

$$A_{\nu n} = S_{fi}\frac{1}{T}\int_0^T D_{\rm el}(\boldsymbol{R}_0, t)e^{i(E_{Nf}-E_{i\nu})t}dt, \tag{13}$$

where the bound-continuum Franck-Condon factor S_{fi} and the electronic matrix element $D_{\rm el}(\boldsymbol{R}_0, t)$ is given by

$$S_{fi} = \int_0^\infty \chi_f^*(R)\chi_{i\nu}(R)dR, \tag{14}$$

$$D_{\rm el}(\boldsymbol{R}_0, t) = \int \phi_f^*(\boldsymbol{r}, t)\boldsymbol{r}\cdot\boldsymbol{F}\,\phi_i(\boldsymbol{r}, \boldsymbol{R}_0)d^3\boldsymbol{r}. \tag{15}$$

We have tested the validity of the Franck-Condon approximation in the evaluation of the bound-continuum matrix element and found it to be accurate, especially for small ν.

The evaluation of the matrix element is conveniently carried out in spherical coordinates [24]. The first step is to rewrite the expression as

$$D_{\rm el}(\boldsymbol{R}_0, t) = \left(E_{i\nu} - E_{Nf} - \frac{\boldsymbol{k}(t)^2}{2}\right) \times \exp\left[i\int_{-\infty}^{t}\frac{\boldsymbol{k}(t')^2}{2}dt'\right]\tilde{\phi}_{i\nu}(\boldsymbol{k}(t), \boldsymbol{R}_0), \tag{16}$$

where we have used

$$-i\frac{\partial\phi_f^*}{\partial t} = \left[\frac{p^2}{2} + \boldsymbol{r}\cdot\boldsymbol{F}\right]\phi_f^*, \tag{17}$$

and $\tilde{\phi}_i$ denotes the Fourier transform of the electronic wave function,

$$\tilde{\phi}_i(\boldsymbol{k}(t), \boldsymbol{R}_0) = \int \exp[-i\boldsymbol{k}(t)\cdot\boldsymbol{r}]\phi_i(\boldsymbol{r}, \boldsymbol{R}_0)d^3\boldsymbol{r}. \tag{18}$$

In the length gauge formulation of the SFA, the transition amplitude only depends on the asymptotic form of the coordinate space initial electronic state [23,24,31,32]. In the laboratory fixed frame this electronic wave function for nuclear orientation $\boldsymbol{R}_0$ reads

$$\phi_i(\boldsymbol{r}, \boldsymbol{R}_0) = r^{(2/\kappa-1)}\exp(-\kappa r)\sum_{l,m} C_{l0}D_{m0}^{(l)}(\hat{\boldsymbol{R}}_0)Y_{lm}(\hat{r}), \tag{19}$$

with C_{l0} asymptotic expansion coefficients [33], and

$$\kappa = \sqrt{2\left(\frac{1}{R_0} - \epsilon_i\right)}, \tag{20}$$

where ϵ_i is the eigenvalue of the electronic Hamiltonian including the nuclear repulsion. In Eq. (19), $D_{m0}^{(l)}(\hat{\boldsymbol{R}}_0)$ is the Wigner rotation function that effects the transformation from the molecular to the laboratory fixed frame.

Finally, the electronic matrix element can be found as

$$D_{\rm el}(\boldsymbol{R}_0, t) = \left(E_{i\nu} - E_{Nf} - \frac{\boldsymbol{k}(t)^2}{2}\right)\exp\left[i\int_{-\infty}^{t}\frac{\boldsymbol{k}(t')^2}{2}dt'\right] \times 4\pi\sum_{l,m}(-i)^l C_{l0}D_{m0}^{(l)}(\hat{\boldsymbol{R}}_0)Y_{lm}(\hat{k}) \times \int_0^\infty j_l(kr)r^{(2/\kappa-1)}\exp(-\kappa r)r^2 dr. \tag{21}$$

The radial integral has a closed analytic form in terms of Gauss's hypergeometric function [34]. The time integration is performed numerically, along with the sum over the number of photons. In the experimental spectra, the protons resulting from dissociative ionization are collected over a range of ejection angles, with respect to the polarization direction. Averaging over the different orientations of the mo-

lecular axis is equivalent, within the axial-recoil model, to summing over the ejected proton directions described by the rotation matrices. This finally reduces to an energy-differential electronic rate, $\Gamma_\nu(E_{Nf})$,

$$\Gamma_\nu(E_{Nf}) = q \int d\hat{\boldsymbol{q}} \sum_{n=n_0}^{\infty} \frac{1}{(2\pi)^2} \times \left| \frac{1}{T} \int_0^T D_{\mathrm{el}}(R_0,t) e^{i(E_{Nf}-E_{i\nu})t} dt \right|^2. \quad (22)$$

To obtain the total rate we use Eqs. (12) and (13), i.e., we multiply by the Franck Condon factor

$$\frac{dw_\nu}{dE_{Nf}} = |S_{fi\nu}(E_{Nf})|^2 \Gamma_\nu(E_{Nf}) \quad (23)$$

and sum over the different initial states

$$\frac{dw}{dE_{Nf}} = \sum_\nu P_\nu \frac{dw_\nu}{dE_{Nf}}. \quad (24)$$

As discussed below, the values of P_ν are determined by the formation mechanism of the ion.

To compare with experimental data, we average over the pulse profile, $f(t)$ [Eq. (1)], which is taken to be Gaussian profile. Under the assumption that the variation in the pule envelope is slow compared with the optical period, the definition of ionization rate for fixed A_0 is still valid. The ionization process can be significant for intense pulses, and thus we should allow for depletion of the molecular state. To model this process, the total ionization probability is found by integrating the rate over time

$$P_I(E_{Nf}) = \sum_\nu \int_{-\infty}^{\infty} \frac{dw_\nu(t)}{dE_{Nf}} N_\nu(t) dt. \quad (25)$$

Here $N_\nu(t)$ denotes the population in a given vibrational state ν. This population can be found from the rate equation:

$$\frac{dN_\nu(t)}{dt} = -\Gamma^\nu_{\mathrm{tot}} N_\nu(t), \quad (26)$$

with the boundary condition $N_\nu(-\infty)=P_\nu$ and $\Gamma^\nu_{\mathrm{tot}}$ denoting the total rate of ionization from the vibrational state ν. By integrating the differential rate over all final states this rate is found as

$$\Gamma^\nu_{\mathrm{tot}} = \int_0^\infty \frac{dw_\nu(t)}{dE_{Nf}} dE_{Nf}. \quad (27)$$

III. RESULTS

In Figs. 1(a) and 1(c) we show the predicted single-proton kinetic energy spectra for Coulomb explosion of H_2^+ [Fig. 1(a)] and D_2^+ [Fig. 1(c)] following strong-field ionization of the neutral, in cases where experimental data for sufficiently short pulses are available. As a first approximation we assume, in obtaining the theoretical results, the initial vibrational states to be populated according to a Franck-Condon distribution. The Frank-Condon factors for the transition $H_2 \rightarrow H_2^+$ ($D_2 \rightarrow D_2^+$) are available in the literature [35].

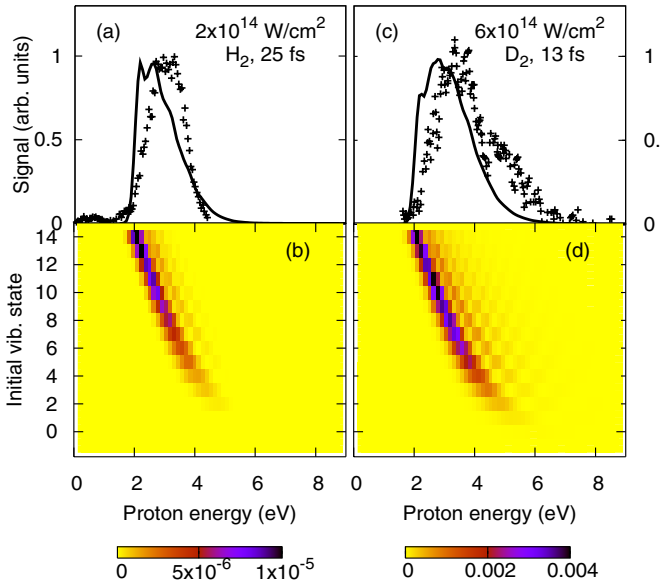

FIG. 1. (Color online) The predicted single-proton spectrum (full curve) for Coulomb explosion of H_2^+ and D_2^+ following strong-field ionization of H_2 and D_2 using 790 nm pulses and assuming an initial Frank-Condon distribution over vibrational states. Peak intensity and duration (FWHM) is given in the figures. We also include the experimental results (crosses) obtained with these pulses in [17] (a) and [22] (c), respectively. Panels (b) and (d) show the contributions to the overall spectrum from the different initial vibrational states. The darker the shading the larger the contribution to a given final proton energy from a particular initial vibrational level.

The theoretical spectrum shown by the full curve in Fig. 1(a) corresponds to a pulse duration of 25 fs (FWHM) and a peak intensity of 2×10^{14} W/cm^2 and is plotted along with experimental results (crosses) for pulses with these characteristics [17]. The molecular ions were created by strong-field ionization of H_2 earlier in the pulse.

Figure 1(c) shows the results for D_2^+ for a pulse duration of 13 fs (FWHM) and a peak intensity of 6×10^{14} W/cm^2 corresponding to the pulse parameters of a very recent measurement [22]. In the experiment [22] a pump was used to generate the molecular ions by photoionization of D_2 and a probe delayed by 591 fs caused the Coulomb explosion. The agreement between the present theory and both experiments is quite convincing, with only a small overestimation of slow protons by theory.

To explain the structure of the theoretical spectra we study the contributions from the different initial vibrational states. Since each component contributes incoherently in the present model, they can be studied in isolation, and we plot in Figs. 1(b) and 1(d) these contributions to the overall spectrum. Here we see that every vibrational state contributes with a peaked structure, dominated by a single peak located at lower energies corresponding to higher excitations.

How this structure of the contributions comes about can be seen by examining the initial and final nuclear wave functions. In Fig. 2(a) the probability densities of two energy-

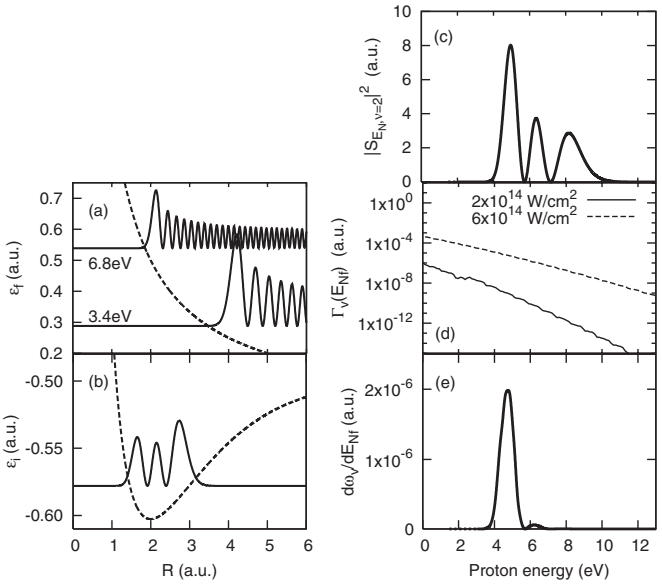

FIG. 2. Calculations showing the result for ions in a vibrational excited initial state with $\nu=2$. The initial and final wave functions squared are shown in (a) and (b). The energies written in (a) indicate the proton energy that the particular states correspond to (i.e., one-half of the total kinetic energy release). Panel (c) shows the Franck-Condon overlap between the initial vibrational state and the final Coulomb wave for the internuclear coordinate. Panel (d) shows the electronic ionization rate for two different intensities and panel (e) shows the ionization probability using pulses of 25 fs duration (FWHM), 790 nm wavelength, and a peak intensity of 2.0×10^{14} W/cm^2, again for $\nu=2$.

normalized continuum states of H_2^+ are presented, along with the density of the $\nu=2$ state in Fig. 2(b). The well-known structure of $\nu+1$ peaks with large probabilities near the classical turning points is clearly seen. Since we have a continuum of final states which are all peaking at different internuclear separations, this initial structure is reflected in the Franck-Condon overlap $S_{fi\nu}(E_{Nf})$ shown in Fig. 2(c). Remember that large internuclear separations R correspond to low energies. In Fig. 2(d) we show the electronic transition rates for two different intensities. The rates decay, roughly exponentially, with increasing ejected proton energy with an attenuation more pronounced for the higher intensity. When multiplying the Franck-Condon factors and the electronic transition rates and integrating over time we obtain the final result for the $\nu=2$ case in Fig. 2(e). The influence of the Franck-Condon factor is still apparent but the attenuation produced by the decrease in electronic transition rate suppresses all but the low energies in the proton spectrum. This is reflected in Figs. 1(b) and 1(d), which isolate the contribution of the different vibrational states weighted by their populations. The dominant peak in the contribution is moved towards lower energies as the molecular ion becomes vibrational excited, reflecting the structure of the nuclear wave function showing a classical turning point at a larger nuclear separation.

When we compare Figs. 1(b) and 1(d) we notice a shift of the kinetic energy distribution towards higher energy both in experiment and theory. In the figures (i) the molecules, (ii) the pulse durations, and (iii) the intensities are different. The difference in Figs. 1(b) and 1(c) can be mainly attributed to (iii) the difference in intensity. The reason is that (i) there is only a small narrowing—far less than needed in order to explain the shift—of the vibrational wave functions when going from H_2^+ to D_2^+. Furthermore, (ii) the pulse duration is so short that only a small portion of the molecular ions are ionized with the present SFA theory (see the scale indicated on the color bar in the bottom of the figure). This means that in Fig. 1(d) a change of the pulse duration from 13 fs to 25 fs only affects the overall yield and not the shape of the spectrum. The change in the result from Fig. 1(a) to 1(c) is hence largely due to the intensity difference. When the intensity is raised the relative difference in electronic rates for different final nuclear energies is lowered and each vibrational state contributes with a broader signal. Furthermore, a combination of the increase in the high-order multiphoton ionization rate and the relatively larger population in the lower ν states compared to the higher ν states, leads to a movement of the bulk of the Coulomb explosion yields towards less excited vibrational states. Both these factors move the resulting spectrum towards higher proton energies when the intensity is increased in agreement with the trend observed in experiments [16,18].

As seen from the discussion above the proton kinetic energy spectrum is very sensitive to the initial distribution over vibrational states. Even though the Franck-Condon distribution used in Fig. 1 only allow for a small portion of the molecular ions to be in the highly excited vibrational states, it is still these states that contributes the most [see Figs. 1(b) and 1(d)]. In Fig. 3(b) we plot the proton spectrum for the exact same pulse as in Fig. 1(a) but using an initial wave function with slightly lower population in the vibrational states with $\nu=9-14$. Making this small adjustment gives perfect agreement with the experiments. In the case of D_2^+ the agreement between theory and experiment is perfect [see Fig. 3(e)] when using the non-Frank-Condon distribution of Fig. 3(d). Experiment [25] and theory [26,27] indicate that such a distribution shifted towards lower vibrational states is naturally produced when the molecular ions are formed upon strong-field ionization of the neutral. This underlines the importance of knowing the initial vibrational distribution when predicting proton spectra.

A. Results using tunneling

To complete the discussion of Coulomb explosion of H_2^+ and D_2^+ the results using simple tunneling models are given. Here the frequency dependence of the field is neglected, and the laser is treated as a slowly varying (quasistatic) electric field that produces tunneling ionization. Strictly speaking, this static model is only valid when the tunneling time is much shorter than the optical cycle as expressed by $\gamma_K \ll 1$, where $\gamma_K=\sqrt{I_P/(2U_P)}$ is the Keldysh parameter. For $I=2\times10^{14}$ W/cm^2, $\gamma_K\sim1.1$, while for $I=6\times10^{14}$ W/cm^2, $\gamma_K\sim0.66$.

In the tunneling limit the ionization rate at a specific nuclear separation is given as [33]

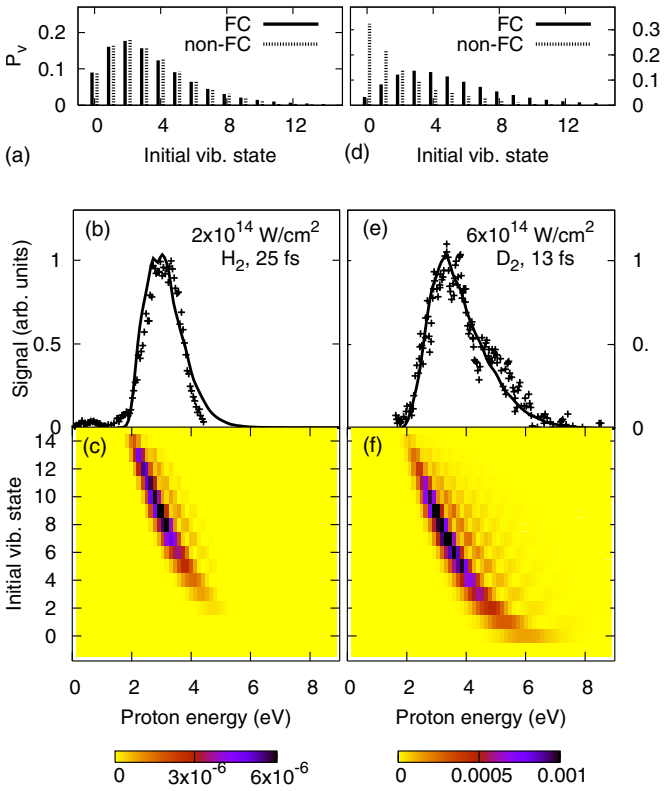

FIG. 3. (Color online) As Fig. 1, but using a non-Franck-Condon distribution over vibrational states for both H_2^+ and D_2^+. Panels (a) and (d) show the Franck-Condon (FC) distribution used in Fig. 1 and the non-Franck-Condon (non-FC) distribution used here.

$$\Gamma_{\text{tun}}(R) = \sum_m \left(\frac{3F_0}{\pi\kappa^3}\right)^{1/2} \frac{B^2(m)}{2^{|m|}|m|!} \frac{1}{\kappa^{2Z/(\kappa-1)}} \left(\frac{2\kappa^3}{F_0}\right)^{2Z/\kappa-|m|-1} \times \exp\left(\frac{-2\kappa^3}{3F_0}\right), \tag{28}$$

where F_0 is the electric field amplitude, $Z=2$ for both H_2^+ and D_2^+, $\kappa=\sqrt{2I_p(R)}$ and

$$B(m) = \sum_l C_{l0} D^l_{m0}(R)(-1)^m \sqrt{\frac{(2l+1)(l+|m|)!}{2(l-|m|)!}}. \tag{29}$$

According to [33] the effect of nuclear motion is included by weighting the electronic ionization rate at different internuclear separations with the probability of being at this separation (the reflection principle),

$$\frac{dw}{dR} = \Gamma_{\text{tun}}(R)|\chi_i(R)|^2. \tag{30}$$

This result can be translated into a function of the proton kinetic energy by assuming that all the Coulomb energy between the two protons at the time of ionization is translated into proton ejection energy. Using $dE_{Nf}/dR=-1/R^2$ we obtain

$$\frac{dw}{dE_{Nf}} = [\Gamma_{\text{tun}}(R)|\chi_i(R)|^2R^2]_{R=1/E_{Nf}}. \tag{31}$$

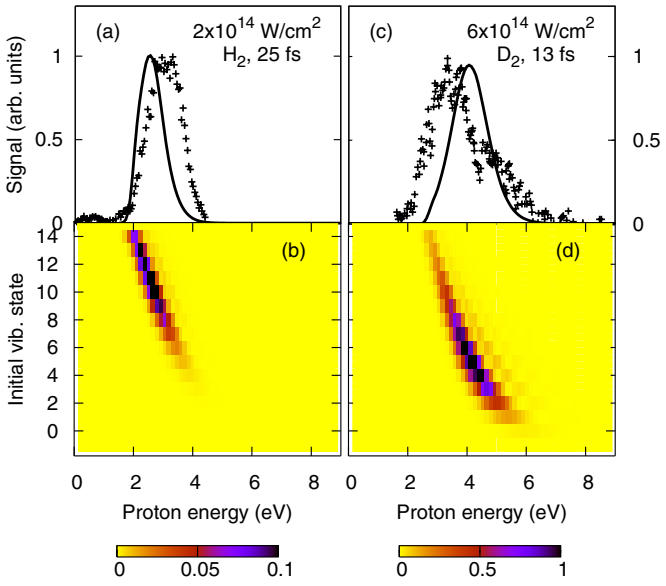

FIG. 4. (Color online) As Fig. 1, but now using the tunneling theory of Ref. [33].

Results are given in Fig. 4 using a Franck-Condon distribution over initial vibrational states. Compared to the strong-field approximation the agreement with experiments is not as good. The spectrum for H_2^+ is moved towards lower energies due to the exponential favoring of the low energy part as typical for a tunneling theory, while the spectrum for D_2^+ is moved towards higher energies. The reason for this unexpected shift is found in the overall larger rates given by tunneling theory resulting in saturation for the highly excited vibrational states. The bulk of the Coulomb explosion yield now comes from less excited states moving the spectrum towards higher energies than actually measured. This rules out the possibility to obtain agreement with experiments by assuming another initial distribution since this assumption,

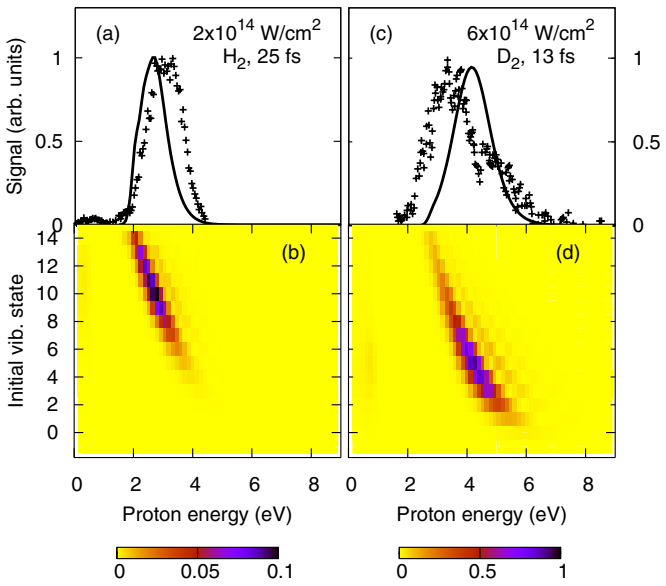

FIG. 5. (Color online) As Fig. 1, but now using the tunneling theory of Ref. [25].

according to the discussion in the last section, favors fast protons. It is still possible to obtain agreement in the case of H_2^+ by changes in the vibrational initial distribution similar to those made using the strong field approximation.

Another way of using tunneling theory to describe Coulomb explosion of H_2^+ is to include the effect of nuclear motion as described in Ref. [25]. The overall rate is here found by

$$\frac{dw}{dE_{Nf}} = \left| \int \chi_f(R)\Gamma_{\text{tun}}^{1/2}(R)\chi_i(R)dR \right|^2. \quad (32)$$

The results are given in Fig. 5, and show to be very similar to the results obtained using the reflection principle (31).

IV. CONCLUSION

In this work, we have presented a relatively simple quantum mechanical model to describe Coulomb explosion of H_2^+ and D_2^+. The model builds on the length gauge molecular strong-field approximation and the predicted proton kinetic energy spectrum shows good resemblance with experiment. Calculations, however, predict the dominant proton emission at slightly lower energies than experimentally measured. The agreement between theory and experiment is perfect when considering a non-Frank-Condon initial vibrational distribution.

The strong-field approximation allows very simple and fast calculations and might, for that reason, be a useful tool in the further understanding of molecular dynamics, including related intense field processes as, e.g., high-harmonic generation. For all purposes it is important only to use the model in the regime, where it is valid, namely describing pulses of high intensities and short durations. If the pulse duration exceeds a few times the vibrational timescale the molecular ion will have time to dissociate and the resulting proton kinetic energy spectrum will move to considerably lower energies.

For comparison, we have discussed the predictions from two different tunneling models, and found less good agreement with experiments.

ACKNOWLEDGMENTS

We thank Thomas Kim Kjeldsen for useful discussions. L.B.M. thanks Xavier Urbain for discussions on the distribution over vibrational levels and the University of Louvain-La-Neuve for hospitality and support. The present work was supported by the Danish Research Agency (Grant. No. 2117-05-0081).

[1] A. Giusti-Suzor, F. H. Mies, L. F. DiMauro, E. Charron, and B. Yang, J. Phys. B **28**, 309 (1995).
[2] J. F. McCann and J. H. Posthumus, Philos. Trans. R. Soc. London, Ser. A **357**, 1309 (1999).
[3] J. H. Posthumus, Rep. Prog. Phys. **67**, 623 (2004).
[4] T. Zuo and A. D. Bandrauk, Phys. Rev. A **52**, R2511 (1995).
[5] L.-Y. Peng, D. Dundas, J. F. McCann, K. T. Taylor, and I. D. Williams, J. Phys. B **36**, L295 (2003).
[6] K. C. Kulander, F. H. Mies, and K. J. Schafer, Phys. Rev. A **53**, 2562 (1996).
[7] D. Pavicic, A. Kiess, T. W. Hnsch, and H. Figger, Eur. Phys. J. D **26**, 39 (2003).
[8] D. Pavicic, Ph.D. thesis, Max Planck Institute of Quantum Optics, 2004.
[9] D. Pavicic, A. Kiess, T. W. Hansch, and H. Figger, Phys. Rev. Lett. **94**, 163002 (2005).
[10] I. Ben-Itzhak, P. Q. Wang, J. F. Xia, A. M. Sayler, M. A. Smith, K. D. Carnes, and B. D. Esry, Phys. Rev. Lett. **95**, 073002 (2005).
[11] I. Ben-Itzhak, P. Wang, J. Xia, A. M. Sayler, M. A. Smith, J. Maseberg, K. D. Carnes, and B. D. Esry, Nucl. Instrum. Methods Phys. Res. B **233**, 56 (2005).
[12] B. D. Esry, A. M. Sayler, P. Q. Wang, K. D. Carnes, and I. Ben-Itzhak, Phys. Rev. Lett. **97**, 013003 (2006).
[13] P. Q. Wang, A. M. Sayler, K. D. Carnes, J. F. Xia, M. A. Smith, B. D. Esry, and I. Ben-Itzhak, Phys. Rev. A **74**, 043411 (2006).
[14] T. Ergler, A. Rudenko, B. Feuerstein, K. Zrost, C. D. Schröter, R. Moshammer, and J. Ullrich, J. Phys. B **39**, S493 (2006).
[15] A. Staudte *et al.*, Phys. Rev. Lett. **98**, 073003 (2007).
[16] A. Rudenko, B. Feuerstein, K. Zrost, V. L. B. de Jesus, T. Ergler, C. Dimopoulou, C. D. Schröter, R. Moshammer, and J. Ullrich, J. Phys. B **38**, 487 (2005).
[17] T. Ergler, A. Rudenko, B. Feuerstein, K. Zrost, C. D. Schroter, R. Moshammer, and J. Ullrich, Phys. Rev. Lett. **95**, 093001 (2005).
[18] C. Beylerian, S. Saugout, and C. Cornaggia, J. Phys. B **39**, L105 (2006).
[19] F. Légaré, K. F. Lee, A. D. Bandrauk, D. M. Villeneuve, and P. B. Corkum, J. Phys. B **39**, S503 (2006).
[20] S. Saugout and C. Cornaggia, Phys. Rev. A **73**, 041406 (2006).
[21] A. Rudenko, T. Ergler, B. Feuerstein, K. Zrost, C. Schroter, R. Moshammer, and J. Ullrich, Chem. Phys. **329**, 193 (2006).
[22] D. S. Murphy, J. McKenna, C. R. Calvert, W. A. Bryan, E. M. L. English, J. Wood, I. C. E. Turcu, W. R. Newell, I. D. Williams, and J. F. McCann, J. Phys. B **40**, S359 (2007).
[23] T. K. Kjeldsen and L. B. Madsen, J. Phys. B **37**, 2033 (2004).
[24] T. K. Kjeldsen and L. B. Madsen, Phys. Rev. A **71**, 023411 (2005).
[25] X. Urbain, B. Fabre, E. M. Staicu-Casagrande, N. de Ruette, V. M. Andrianarijaona, J. Jureta, J. H. Posthumus, A. Saenz, E. Baldit, and C. Cornaggia, Phys. Rev. Lett. **92**, 163004 (2004).
[26] T. K. Kjeldsen and L. B. Madsen, Phys. Rev. Lett. **95**, 073004 (2005).
[27] A. Requate, A. Becker, and F. H. M. Faisal, Phys. Rev. A **73**, 033406 (2006).
[28] L.-Y. Peng, I. D. Williams, and J. F. McCann, J. Phys. B **38**, 1727 (2005).
[29] D. Brink and G. Satchler, *Angular Momentum* (Oxford Univer-

sity Press, London, 1968).
[30] R. Zare, *Angular Momentum* (Wiley, New York, 1988).
[31] G. F. Gribakin and M. Y. Kuchiev, Phys. Rev. A **55**, 3760 (1997).
[32] T. K. Kjeldsen, C. Z. Bisgaard, L. B. Madsen, and H. Stapelfeldt, Phys. Rev. A **71**, 013418 (2005).
[33] X. M. Tong, Z. X. Zhao, and C. D. Lin, Phys. Rev. A **66**, 033402 (2002).
[34] I. S. Gradshteyn and I. M. Ryzhik, *Table of Integrals, Series, and Products* (Academic, San Diego, 1994).
[35] G. H. Dunn, J. Chem. Phys. **44**, 2592 (1966).